An Enhanced DC Voltage Droop-Control for the VSC–HVDC Grid

Haifeng Li, *Student Member, IEEE*, Chongru Liu, *Senior Member, IEEE*, Gengyin Li, *Member, IEEE*, and Reza Iravani, *Fellow, IEEE*

***Abstract*—This paper introduces an enhanced droop-based dc-voltage control method, including dead-band, for applications to the high-voltage direct-current (HVDC) grid that utilizes the voltage-sourced converter (VSC) technology. The proposed droop-control structure also autonomously imposes energy balance between the HVDC grid and its host ac system. The droop-control method (1) divides the VSC stations into four groups, (2) activates the droop-control of each group based on a prespecified voltage margin, and (3) introduces an improved power-voltage characteristic for desirable VSC station dynamic performance. Feasibility and performance of the proposed control method are evaluated based on time-domain simulation studies in the PSCAD platform, using the IEEE-39-Bus system that imbeds a five-terminal VSC–HVDC grid. Each VSC station is a monopolar modular multilevel converter (MMC). The study results show that the proposed droop-control method enables the HVDC-AC system to reach a new steady state after transient events.**

***Index Terms*—Modular multilevel converter, dc voltage droop-control, dead-band droop-control, VSC–HVDC grid.**

I. Introduction

ECONOMICAL feasibility and technical features of the voltage-sourced converter (VSC) [1]–[3] technology, and particularly those of the modular-multilevel converter (MMC) [4]–[6] configuration, have made the concept of HVDC grid a reality [7], [8]. One of the challenges and active research and development aspects of the VSC-based HVDC grid is the DC-side voltage/power control, i.e., simultaneously (i) the DC node voltages must be maintained within a permissible range and (ii) the net-zero exchange of power between the DC grid and its AC host system(s) must be imposed [9]–[11].

The HVDC grid voltage control is achieved by: either (i) a centralized DC voltage control method which requires an extensive and fast communication infrastructure [9] or (ii) a distributed droop-based DC voltage control which exploits local voltages and eliminates the need for fast communication [12]–[14]. The focus of this paper is the latter method.

To ensure coordinated operation and retention of viable operating points of the HVDC converter stations, the droop-control can be realized based on:

1) Voltage Dead-band [15]: When the operating point of a converter station is within the dead-band, constant current/power control mode is adopted. Otherwise, the droop-control, based on a unique droop ratio, is activated. The challenges of this method include (i) determination of a unique and feasible dead-band for each converter station within a fairly narrow voltage range, i.e., $\pm 10\%$, and (ii) the need to re-determine each dead-band as the number of converter station changes, i.e., due to the grid expansion or when a converter station is out-of-service.
2) Voltage Undead-band [16]: The undead-band droop-control introduces multiple droop ratios, one per converter station, and abandons the constant current/power control mode of the dead-band approach. This method can optimize dynamic performance of the droop-control [9], however, (i) requires engineering judgement to properly select the droop ratios and (ii) the operating points of converters are subjected to excursions after transient events.

This paper presents an enhanced, dead-band-based, DC voltage droop-control for the MMC-HVDC grid. The numbers of voltage margins and dead-bands in the proposed method are not affected by the number of converter stations. The proposed approach divides the MMC-HVDC stations in four groups. Each converter group is assigned with (i) a pre-specified priority for activating the droop control and (ii) a unique voltage margin and voltage dead-band. Thus changes in the number of the operational converter stations, i.e., addition of a new station or out-of-service mode of a station, are accommodated based on the existing dead-bands. Subsequent to a transient event, the dead-band droop-control of the MMCs within a lower-priority group can be de-activated so that the MMCs can maintain their pre-disturbance operating points. Since the active power of a converter station intends to decrease due to the current limits, a single droop ratio based on reducing the active power is adequate for this approach.

The rest of this paper is organized as follows. Section II introduces the proposed droop-control. Section III describes the converter grouping approach. Section IV explains the voltage margins, the dead-bands and the improved power-voltage

Manuscript received February 18, 2016; revised April 27, 2016; accepted June 1, 2016. Date of publication June 7, 2016; date of current version February 16, 2017. This work was supported by the National Natural Science Foundation of China under Grant 51277068 and the Program for New Century Excellent Talents in University under Grant NCET-12-0846, and in part by "111" Project of China under Grant B08013 and the 863 Program under Grant 2015AA050101. Paper no. TPWRS-00269-2016.

H. Li, C. Liu, and G. Li are with the State Key Laboratory for Alternate Electrical Power System with Renewable Energy Sources, North China Electric Power University, Beijing 102206, China (e-mail: haifeng633@sina.com; chongru.liu@ncepu.edu.cn; ligy@ncepu.edu.cn).

R. Iravani is with the Department of Electrical and Computer Engineering, University of Toronto, Toronto, ON M5S3G4, Canada (e-mail: iravani@ecf.utoronto.ca).

Color versions of one or more of the figures in this paper are available online at http://ieeexplore.ieee.org.

Digital Object Identifier 10.1109/TPWRS.2016.2576901

0885-8950 © 2016 IEEE. Personal use is permitted, but republication/redistribution requires IEEE permission.
See http://www.ieee.org/publications_standards/publications/rights/index.html for more information.

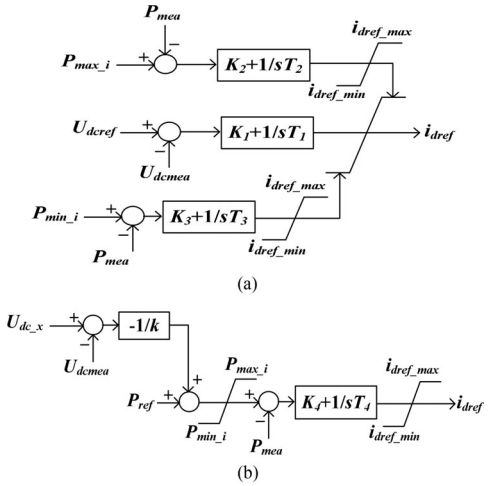

Fig. 1. Outer-loop current controllers in *d*-axis of the dead-band droop-control: (a) DC-side voltage control, and (b) active power control.

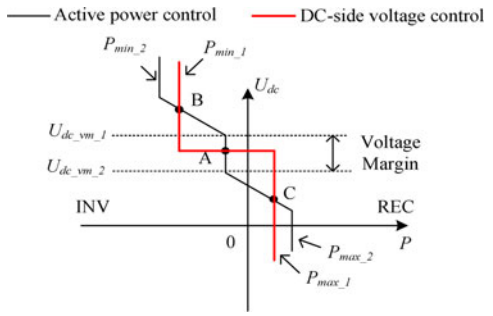

Fig. 2. The conventional $P - U_{\rm dc}$ characteristics of the DC-side voltage control and active power control.

characteristic. Section V provides the PSCAD-based study results and Section VI presents the conclusions.

II. Dead-Band Droop-Control

The conventional *dq*-current control [17], [18] is the widely used approach for droop-based control of the DC-side voltage. Fig. 1(a) and(b) show the outer-loop *d*-axis controller that generates $i_{\rm dref}$ based on real power or DC-side voltage, respectively [9]. Fig. 2 shows the conventional power-voltage $(P - U_{\rm dc})$ characteristics [9] that impose the cooperation between the DC-side voltage control of Fig. 1(a) and the active power control of Fig. 1(b).

In Fig. 1, $P_{\max\_i}(P_{\min\_i})$ is the maximum (minimum) of real power of the corresponding converter where subscript *i* refers to the controller type, i.e., $i = 1$ is the DC-side voltage control and $i = 2$ is the active power control. $i_{\rm dref\_max}(i_{\rm dref\_min})$ defines the top (bottom) straight-line characteristic of $i_{\rm dref}$. $P_{\rm ref}(U_{\rm dcref})$ is the steady-state reference value of active power (DC-side voltage) and $P_{\rm mea}(U_{\rm dcmea})$ is the measured value. K_j and T_j are gains and time-constants of the PI controllers, where $j = 1$, 2, 3 and 4. The $P - U_{\rm dc}$ characteristics of Fig. 2 show that $U_{\rm dc\_x}$ of Fig. 1(b) can be $U_{\rm dc\_vm\_1}$ or $U_{\rm dc\_vm\_2}$ in Fig. 2. *k* in Fig. 1(b) refers to the slope of each segment of the $P - U_{\rm dc}$ of Fig. 2 when the active power is within the range $(P_{\min\_2}, P_{\max\_2})$.

Fig. 2 reveals that within the voltage margin, one controller provides constant voltage control and the other one determines the active power. Point "A" on Fig. 2 is the steady state equilibrium point where $(P_{\rm ref}, U_{\rm dcref})$ locates. When the DC voltage exceeds the voltage margin in Fig. 2, a droop-control is applied by the "*P* control" and the original "$U_{\rm dc}$ control" behaves as a constant active power control. Thus the updated steady-state point migrates to either point B or C on Fig. 2.

In general, the slope for "A to B" can be different from that of "A to C". The reason is that the absolute value of active power can hardly increase whereas often reduces in practice. Therefore, to determine the slope of the droop-control, it is adequate to consider either "A to B" or "A to C", according to the location of "A". A more desirable $P - U_{\rm dc}$ characteristic and the corresponding method to determine *k* are introduced in Section IV which also discusses the dead-band selection.

III. Converter Groups

This section introduces (i) the basis for dividing the converters of an HVDC grid into four groups by which the desired dynamic behavior and the optimal operating point of each converter are determined, and (ii) the principals that the converter groups cooperate with each other in terms of the overall system control. An HVDC grid includes four or more converter stations [19] and is divided into:

- Group 1 which includes converters (at least one) that control the DC-side voltage (DC slack bus) and equipped with the DC-side voltage control of Fig. 1(a).
- Group 2 and Group 3 which each contains converters which are equipped with the active power control of Fig. 1(b). The converters in Group 2 (Group 3) are connected to strong (weak) AC buses with SCR>2 (SCR<2).
- Group 4 which is formed by converters that do not participate in the DC voltage control.

Group 1 to Group 4 converters are given descending priority for activating the droop-based control. If all converters within a group reach their power limits and the DC voltage fails to retain an acceptable value, then the droop-based control of the converters in the next group are engaged.

Subsequent to a transient scenario, i.e., an *N*-1 contingency event, in the HVDC grid, the new steady-state DC voltage is desired to be within the voltage margins of either Group 1 or Group 2. Therefore, Group 3 and Group 4 converters often are not involved and not affected by the droop-control process. The converters of Group 2 and Group 3 are not recommended to be merged as a single group. The reason is that as a single group, controllers of the MMCs engage and disengage more often subsequent to a transient event and consequently initiate undesirable oscillations and adverse dynamics impacts on the weak AC buses. A converter is desired to reach its maximum and minimum active power limits within its voltage margin. This determines the minimum value of *k* in Fig. 1(b). The converter grouping approach:

- Provides a straight-forward and easy approach for practical implementation and only requires four voltage margins.
- Does not require re-adjustment of voltage margins when new converter stations are introduced in the grid, i.e., inherently accommodates system expansion and out-of-service condition of each converter station.

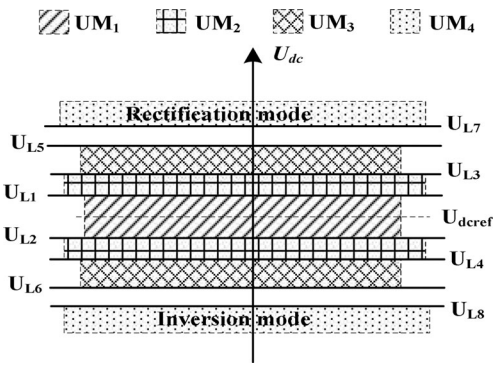

Fig. 3. Voltage margins for the four converter groups.

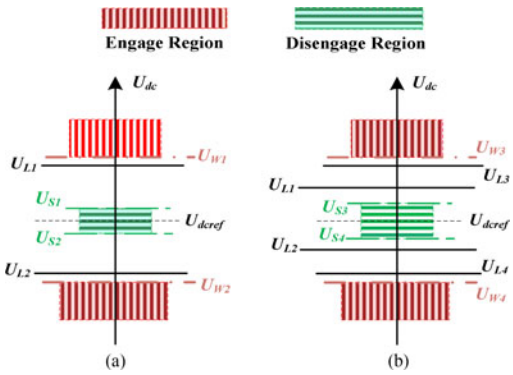

Fig. 4. Engage and disengage regions: (a) Group 2, and (b) Group 3.

- Takes advantage of the range that power of a converter can be varied to balance the active power of the DC grid.
- Assists the converters in the new steady state, when connected to weak AC buses, to converge to their original operating points which are also the optimal operating points.

IV. Dead-Band for Voltage Margin

A. Voltage Margins and Dead-Bands

The priorities of activating the droop-control for Group 1 to Group 4 converters are determined by voltage margins UM_1 to UM_4 formed by different DC voltage values U_{L1} to U_{L8}, shown in Fig. 3. Since margin UM_4 does not share a common boundary with the other margins, it does not require a dead-band. Since Group 4 converters are not involved in the droop-control, when $U_{\rm dc}$ is within the UM_4 margin, MMCs in Group 4 are disconnected from both AC and DC buses. It should be noticed that the upper area of margin UM_4 is only for rectification and the lower one is for inversion. When $U_{\rm dc}$ recovers to $U_{\rm dcref}$ after a transient event, converters in Group 4 are reconnected.

To avoid repeated movement of the operating point between either UM_1 to UM_2 or UM_2 to UM_3, dead-bands are introduced by the "engage" and "disengage" regions of the droop-control for converters in Group 2 and Group 3, as shown in Fig. 4. In Fig. 4, $U_{\rm Wj}(U_{\rm Sj})$ is the DC voltage threshold of the engage (disengage) regions, where subscript j = 1, 2 (3, 4) is for Group 2 (Group 3) converters and the odd (even) number refers to the upper (lower) region. The engage region of Group 2 (Group 3) is the area that $U_{\rm dc} > U_{W1}(U_{W3})$ and $U_{\rm dc} < U_{W2}(U_{W4})$. The disengage region of Group 2 (Group 3) is the area that $U_{S2}(U_{S4}) < U_{\rm dc} < U_{S1}(U_{S3})$. When $U_{\rm dc}$ enters into the engage (disengage) region, the droop-control is activated (de-activated) for the corresponding converters.

For the dead-band of a converter in Group 2 or Group 3, $U_{\rm Wj}$ is around $U_{\rm Lj}(j = 1, 2, 3, 4)$. Since converters intend to reduce the amount of active power, an increasing (decreasing) $U_{\rm dc}$ indicates that the DC grid needs to import (export) less active power from (to) the AC system. Therefore, rectifier (inverter) is more sensitive than the inverter (rectifier) to activate the droop-control, when dealing with an increasing (decreasing) $U_{\rm dc}$. Hence, U_{W1} and U_{W3} can be marginally smaller (greater) than U_{L1} and U_{L3}, respectively, for the rectification (inversion) mode. U_{W2} and U_{W4} could be slightly higher (lower) than U_{L2} and U_{L4}, respectively, for the inversion (rectification) mode.

In Fig. 4(a), U_{S1} and U_{S2} should be close to $U_{\rm dcref}$ and further away from U_{W1} and U_{W2}, respectively. The gap between U_{S1} and U_{S2} should be adequate to cover variations in DC voltage measurement. In Fig. 4(b), $U_{S3}(U_{S4})$ is marginally smaller (greater) than $U_{L1}(U_{L2})$.

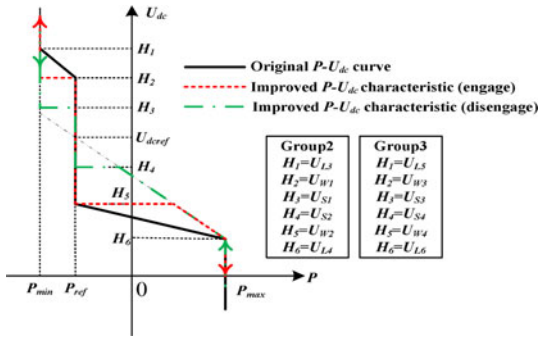

Fig. 5. Comparison of the conventional and improved $P - U_{\rm dc}$ characteristics.

B. Droop Ratios

Fig. 5 compares the original $P - U_{\rm dc}$ characteristic of Fig. 2 and the improved $P - U_{\rm dc}$ characteristic, considering the engage and disengage regions. H_1 to H_6 are different DC voltage values and are not the same for Group 2 and Group 3.

Fig. 5 shows that the improved $P - U_{\rm dc}$ characteristic consists of the engage and disengage parts as discussed in Fig. 4. The main differences between the original and the improved $P - U_{\rm dc}$ characteristics are that (i) the improved $P - U_{\rm dc}$ characteristic enables $U_{{\rm dc}\_x}$ in Fig. 1(b) to set at $U_{\rm dcref}$ rather than H_2 or H_5 and (ii) k in Fig. 1(b) adopts the slope of the segment for which the absolute value of active power reduces. The improved $P - U_{\rm dc}$ characteristic:

- Simplifies the determination process of $U_{{\rm dc}\_x}$ and k, i.e., the original $P - U_{\rm dc}$ characteristic requires to determine if $U_{{\rm dc}\_x} = H_2$ or $U_{{\rm dc}\_x} = H_5$ to obtain the corresponding value of k. Therefore, two values of each of the $U_{{\rm dc}\_x}$ and k in the original $P - U_{\rm dc}$ characteristic are required

for either increasing or decreasing the amount of active power, respectively. However, since the converters intend to reduce the amount of active power in practice, the values of each of the U_{dc_x} and k for decreasing the amount of active power are enough for the droop-control.

- Makes the new steady-state U_{dc} closer to U_{dcref}, i.e., in Fig. 5 when U_{dc} is smaller than H_5, the droop-control is activated. Assuming that the new steady-state active power is zero, the new steady-state $U_{\mathrm{dc}}$of the improved $P-U_{\mathrm{dc}}$ characteristic is between H_4 and H_5 while the new steady-state U_{dc} of the original $P-U_{\mathrm{dc}}$ characteristic is below H_5. Thus the improved $P-U_{\mathrm{dc}}$ characteristic, under droop-control, obtains a new steady-state U_{dc} which is closer to U_{dcref}.

Since U_{dc_x} is set as U_{dcref} in the improved $P-U_{\mathrm{dc}}$ characteristic of Fig. 5, k is calculated based on

$$k=\max\left(\frac{H_1-U_{\mathrm{dcref}}}{P_{\min}-P_{\mathrm{ref}}},\frac{H_6-U_{\mathrm{dcref}}}{P_{\max}-P_{\mathrm{ref}}}\right), \tag{1}$$

which gives the minimum value of k by which the converter can reach $P_{\min}$ and $P_{\max}$ within its voltage margin. In this paper, optimization of k is not discussed. Fig. 5 shows an example that P_{ref} is near $P_{\min}$ and the slope of P_{ref} to $P_{\max}$ determines k. If P_{ref} is near $P_{\max}$, then k is more influenced by the slope of P_{ref} to $P_{\min}$. The two scenarios are covered in (1) by function "max()". The power and voltage in (1) are per unit values.

C. Evaluation of Dead-Bands

This section evaluates the effect of dead-bands on the converter transient performance. Then proper threshold values of the engage and disengage regions for a converter of Group 2 or Group 3, i.e., U_{Wj} and $U_{\mathrm{Sj}}(j=1,2(3,4)$ for a Group 2 (Group 3) converter), are determined based on an objective function by a trial and error approach [20].

- Over-corrections: Assume that x_{ref} is the original steady state value of variable x, and x_F is the first encountered peak of x during a transient event. The over-correction of x is defined as

$$x_O=\left|\frac{x_{\mathrm{ref}}-x_F}{x_{\mathrm{ref}}}\right|. \tag{2}$$

  x_O is mainly affected by U_{W1} to U_{W4} which determine the threshold DC voltage at which the droop-control is activated.
- Adjustment-time: This is the time duration for the system to migrate from the original to the updated steady-state. Therefore, the interactions of the activated droop-control among the converters determine the duration of the adjustment-time. As a result, the values of U_{S1} to U_{S4} in Fig. 4, which de-activate a converter's droop-control, are the key factors to determine the adjustment-time.
- Updated steady-state DC voltage: When the droop-control, using the improved $P-U_{\mathrm{dc}}$ characteristic, is engaged within the voltage margin, the updated steady-state DC voltage can be between the engage and disengage region. For example, when $P=0$ in Fig. 5, U_{dc} is between H_4 and H_5. Since U_{W1} to U_{W4} are determined for obtaining a lower over-correction, $U_{\mathrm{S1}}\sim U_{\mathrm{S4}}$ affect the value of the updated-steady state DC voltage.

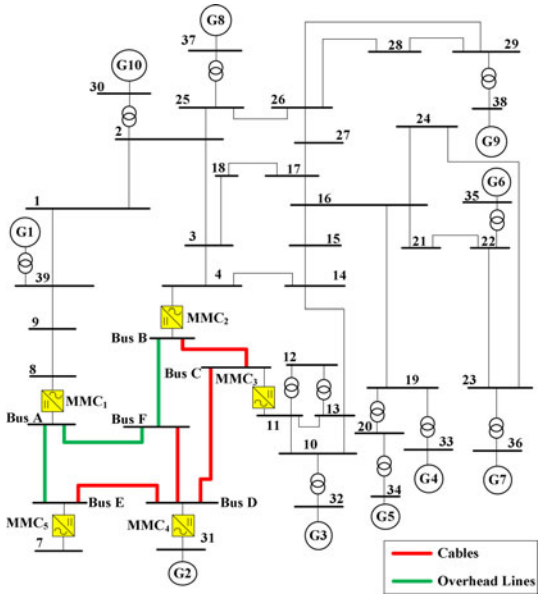

Fig. 6. The test HVDC-AC hybrid system.

TABLE I
STEADY STATE OPERATION POINT AND CIRCUIT PARAMETERS OF MMCS

MMC	1	2	3	4	5
Active Power (MW)	−943.7	−684.6	912.2	990.8	−233.8
Reactive Power (Mvar)	−79.4	−36	63.47	−18	−84
DC voltage (kV)	633	640	645	644.4	642.5
SCR of the AC bus	1.7	7.6	20.3	1.5	–
SM Capacitance (mF)	12	9.63	12	12	2.83
Arm Inductance (mH)	41.66	51.9	41.66	41.66	176.48

Note: SCR is short for short circuit ratio.

V. STUDY RESULTS

A. Test System

The system of Fig. 6 is used as the study system to evaluate and validate the effectiveness of the proposed enhanced droop-control. Fig. 6 shows a modified version of the IEEE-39 Bus system [21], augmented by a five-terminal monopolar MMC-based HVDC grid. The nominal DC voltage of the DC grid is 640 kV. Each MMC is based on 400 sub-modules in each arm and is connected to the corresponding AC bus through a Y/Δ transformer. MMC_3 controls the DC voltage and the other MMCs regulate power flowing into or out of the DC grid. MMC_5 supplies a passive system and MMC_4 is connected to a source, i.e., equivalent of a wind power plant. The DC network includes overhead lines and underground cables. Details of the HVDC grid and its parameters are given in [10] and Table I. The positive direction of power is assumed from the AC side to the DC side.

TABLE II
VOLTAGE MARGINS OF CONVERTER GROUPS

Group 1		Group 2		Group 3		Group 4	
U_{L1}	U_{L2}	U_{L3}	U_{L4}	U_{L5}	U_{L6}	U_{L7}	U_{L8}
1.05	0.97	1.06	0.94	1.1	0.9	–	0.7

TABLE III
DEAD-BANDS OF MMCS

MMC	U_{W1}	U_{W2}	U_{W3}	U_{W4}	U_{S1}	U_{S2}	U_{S3}	U_{S4}
1	–	–	1.065	0.935	–	–	1.035	0.96
2	1.05	0.98	–	–	1.03	0.99	–	–
4	–	–	1.055	0.93	–	–	1.03	0.98

TABLE IV
ACTIVE POWER LIMITS AND DROOP RATIOS OF MMCS

MMC	1	2	3	4
P_{max}(MW)	−400	753	1100	1100
P_{min}(MW)	−1038	−753	−1100	0
Droop Ratio k	−0.17	−0.03	–	−0.1

B. Voltage Margin, Dead-Band and Droop Ratio

According to the SCR values of Table I and the control modes of MMCs, MMC_3 and MMC_2 are classified as Group 1 and Group 2, respectively. MMC_1 and MMC_4 constitute Group 3 and MMC_5 forms Group 4. Voltage margins for the four groups are listed in Table II by which the dead-bands of converters are provided in Table III. Since MMC_5 cannot operate as a rectifier, there is no U_{L7} in Table II. Parameters in Tables II and III are in per unit. The based power and voltage of each MMC is the steady-state value of active power and DC voltage of the corresponding MMC in Table I

Table II indicates that the DC voltage of a converter can vary within $\pm 10\%$ of its steady state value under the droop-control. When DC voltage reduces to 0.7 pu, MMC_5 is disconnected from the system to reduce load and maintain a stable $U_{\rm dc}$. In Table III, $U_{\rm Wj}$ is closed to $U_{\rm Lj}$, where $j = 1, 2, 3$, and 4. To make the droop-control of a rectifier (inverter) more sensitive to an increase (decrease) in $U_{\rm dc}$, in Group 3, U_{W3} and U_{W4} of MMC_1 are greater than those of MMC_4. Table IV gives the pre-specified active power limits and the corresponding k value for each converter based on (1).

C. Performance Evaluation

The objective of this section is to evaluate the performance of the proposed enhanced droop-control during system transients. Initially, the system of Fig. 6 is under a steady-state condition as specified in Table I.

- Case I - Removal of an MMC from service

At time $t = 7$ s, the system is subjected to the removal of MMC_3 (Group 1) from service, i.e., (i) the AC-side circuit breakers open and subsequently (ii) the DC-side is disconnected when the converter DC current reaches zero after about 10 ms. Fig. 7 shows the system response to the transients.

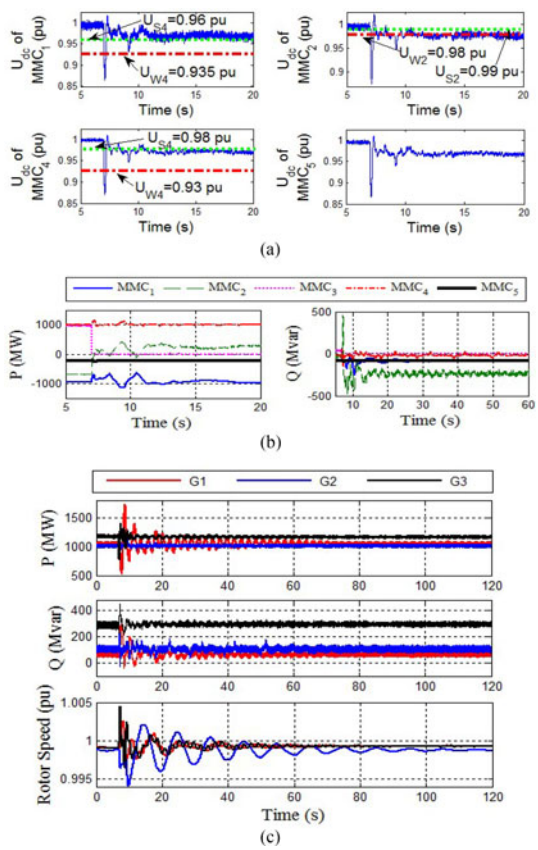

Fig. 7. System response to the removal of MMC_3: (a) DC voltages of MMCs, (b) power of MMCs, and (c) power and rotor speeds of generators.

Fig. 7(a) shows the DC voltages of the MMCs during the transient fault. Due to the disturbance at $t = 7$ s, all DC voltages drop from 1 pu to 0.869 pu which is smaller than the engage region thresholds, that is, U_{W2} of MMC_2 and U_{W4} of MMC_1 and MMC_4. So the droop-controls of the MMCs are activated and the DC voltages increase. $U_{\rm dc}$ of MMC_1 is higher than its disengage region threshold U_{S4} at $t = 7.23$ s and $U_{\rm dc}$ of MMC_4 exceeds its U_{S4} at $t = 7.24$ s. Then the DC voltages of MMC_1 and MMC_4 do not enter their engage regions again and the droop-controls of the two MMCs are de-activated. $U_{\rm dc}$ of MMC_2 enters its engage region or disengage region several times between $t = 7$ s and $t = 11.7$ s. At $t = 11.7$ s, $U_{\rm dc}$ of MMC_2 enters its engage region and after that it does not reaches its disengage region. Therefore, the new steady-state DC voltage of the HVDC grid is controlled by the droop-control of MMC_2. $U_{\rm dc}$ of MMC_5 is always higher than $U_{L8} = 0.7$ pu, under which the Group 4 voltage margin is formed in Table II, and MMC_5 is under normal operation. Fig. 7(a) indicates that the removal of MMC_3 from service does not result in the DC voltage collapse of the system, even in the absence of the DC slack bus, i.e., MMC_3, when the proposed droop-control is utilized.

Fig. 7(b) shows the power transfer of the MMCs during the transient event. At $t = 7$ s, due to the decrease of the DC

voltages, the droop-controls of MMC_1, MMC_2 and MMC_4 are activated and the powers of the MMCs change to stabilize the DC voltage. During the transient state, power of MMC_2 (Group 2) changes more noticeably than that of MMC_1 and MMC_4 (Group 3). This indicates that, as compared with the converters of Group 2, converters of Group 3 are less affected in the transient event. When $U_{\rm dc}$ begins to decrease at $t = 7$ s, in Group 3, the active power of MMC_1 (inverter) changes more drastically than that of MMC_4 (rectifier). This indicates that the converter with the proposed droop-control intends to decrease the amount of power. The HVDC grid reaches to the new steady state after 50 s. MMC_2 regulates the DC voltage subject to the new active and reactive power values, but MMC_1 and MMC_4 recover to their original operating points. Power of MMC_5 (Group 4) remains almost unaffected during the whole process.

Fig. 7(c) shows the dynamics of G1 to G3 of Fig. 6 during the transient scenario. The output powers of G1 and G3 exhibit significant fluctuations but the rotor speed of G2 oscillates more noticeably since G2 is an isolated unit. The power of MMC_4 does not change significantly, therefore, the change of power flow in this case is mainly accommodated by the other generators.

- Case II - DC transmission line trip-out

Under the same initial steady-state as described for Case I, at $t = 7$ s, a line-to-ground fault occurs at the DC transmission line between Bus D and Bus F of Fig. 6. After 1 ms, the fault is detected and the DC transmission line is tripped out by the corresponding DC circuit breakers after another 1 ms [10]. Fig. 8 shows the system response to the transient scenario.

Fig. 8(a) shows that the outage of the DC transmission line results in disturbances in the DC voltages. At $t = 7$ s, $U_{\rm dc}$ of MMC_1 and MMC_2 are going to decrease while $U_{\rm dc}$ of the other MMCs intend to increase. The DC voltage of MMC_1 remains higher than its disengage region threshold U_{S4} and the droop-control of MMC_1 is de-activated during the transient process. $U_{\rm dc}$ of MMC_2 becomes smaller than U_{W2} at $t = 7$ s and enters its engage region. But 0.24 s later, $U_{\rm dc}$ of MMC_2 increases and becomes higher than U_{S2}, which is the threshold of the disengage region of MMC_2. Between $t = 7$ s and $t = 8.68$ s, the DC voltage of MMC_2 repeatedly operates at either the engage region or the disengage region. After $t = 8.68$ s, $U_{\rm dc}$ of MMC_2 operates at its disengage region or the dead-band. Therefore, the droop-control of MMC_2 is de-activated after $t = 8.68$ s. $U_{\rm dc}$ of MMC_4 increases and enters the engage region $(U_{\rm dc} > U_{W3})$ of MMC_4 at $t = 7$ s. However 0.27 s later the DC voltage of MMC_4 becomes lower than U_{S3} (the disengage region threshold) and the corresponding droop-control is de-activated.

As the DC slack bus, MMC_3 tries to prevent the rising DC voltage from 1.034 to 1 pu after the fault. However, MMC_5 does not participate in regulating the DC voltage of the HVDC grid. In this transient process, the droop-controls of MMC_2 and MMC_4 are activated and assist MMC_3 to stabilize the DC voltage of the HVDC grid. At the new steady-state, MMC_2 and MMC_4 de-activate their droop-controls and the DC voltage is regulated by MMC_3.

Fig. 8(b) shows the power transfer of the MMCs during the transient state. Since MMC_2 to MMC_4 cooperate to stabilize the DC voltage, the two MMCs have more noticeable change of power than MMC_1 and MMC_5. After $t = 20$ s, the HVDC grid reaches a new steady state.

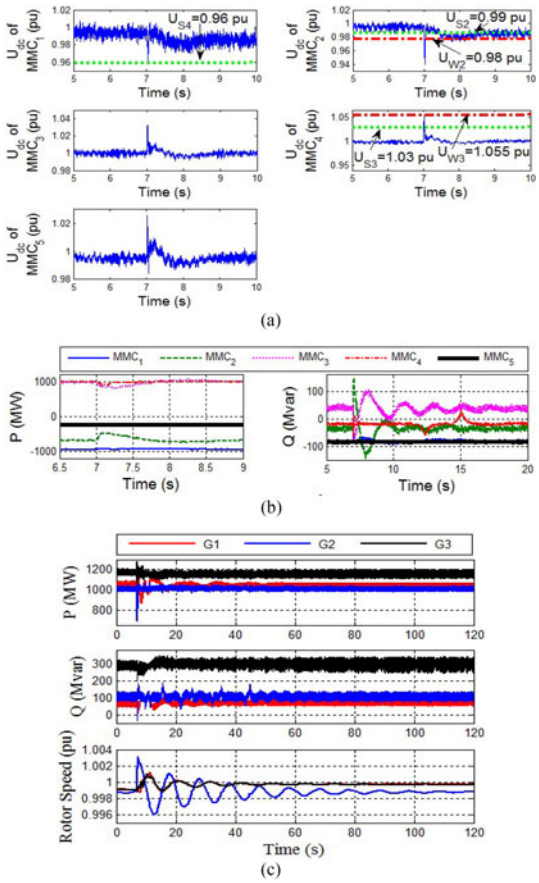

Fig. 8. System response to the outage of DC transmission line: (a) DC voltages of MMCs, (b) power of MMCs, and (c) power and rotor speeds of generators.

Fig. 8(c) shows the generator dynamics during the transient scenario. Since the outage of the DC transmission line only results in power flow redistribution in the HVDC grid, the operating point of the AC system does not change between the pre- and post-disturbance state. Thus the generator dynamics of Fig. 8(c) are less severe than those of Fig. 7(c).

D. Dead-Band Evaluation

This section investigates the effects of the engage and disengage regions of the MMC dead-bands on the over-correction, adjustment-time and new steady state DC voltage, subsequent to a transient event. The thresholds of the lower dead-band of MMC_2 and MMC_1, i.e., U_{W2} and U_{S4} respectively, are selected to demonstrate the procedures to determine the threshold values of the engage and disengage regions of the droop-control. The transient event is the removal of MMC_3, i.e., Case I in part C of Section V.

- Case III – Selection of U_{W2}

U_{W2} is the engage region threshold of the droop-control of MMC_2. By changing the value of U_{W2}, the over-corrections of variable x, given by (2), change. Fig. 9 shows $x_{\rm O}$ for power, DC voltage and current of the MMCs as functions of U_{W2}.

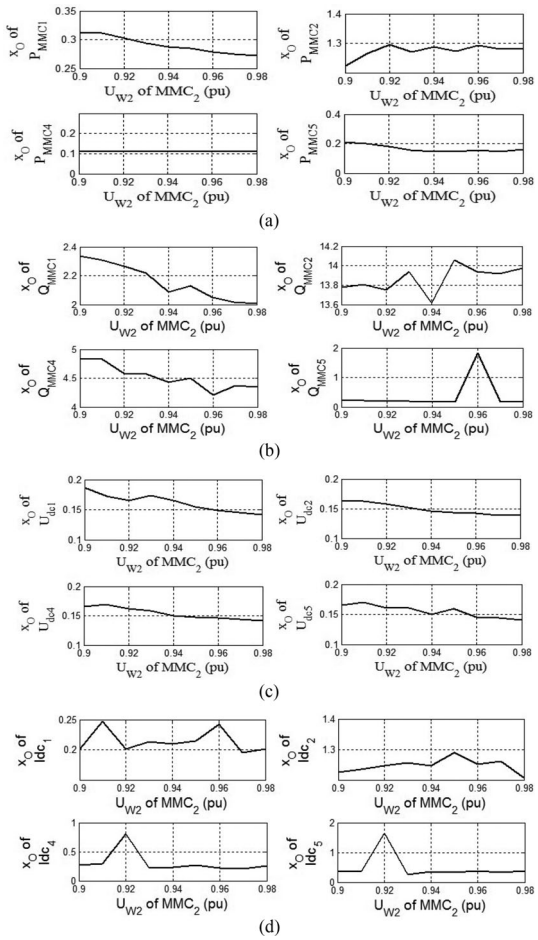

Fig. 9. Over-corrections in transient state of the MMC electric variables: (a) active power, (b) reactive power, (c) DC voltage, (d) DC current.

Fig. 9(a) shows that when $U_{W2} = 0.98$ pu, the x_O of the active power of MMC_2 ($\mathrm{P}_{\mathrm{MMC2}}$) is not at its minimum value while those of MMC_1, MMC_4 and MMC_5 are at their minimum values. This indicates that if $U_{W2} = 0.98$ pu, then the lowest over-corrections occur for the active powers of MMC_1, MMC_4 and MMC_5 in the transient event. The corresponding value of x_O of $\mathrm{P}_{\mathrm{MMC2}}$ is fairly close to its minimum value at $U_{W2} = 0.98$ pu, and the over-correction of $\mathrm{P}_{\mathrm{MMC2}}$ in this transient event is acceptable.

Fig. 9(b) shows the relationship between x_O and U_{W2} for the reactive powers of MMC_1, MMC_2, MMC_4 and MMC_5. Similar to the active power of Fig. 9(a), reactive power of MMC_2 ($\mathrm{Q}_{\mathrm{MMC2}}$) does not obtain the minimum value of the x_O at $U_{W2} = 0.98$ pu where the reactive powers of MMC_1, MMC_4 and MMC_5 reach to their minimum values. As a result, over-corrections of the reactive powers of MMC_1, MMC_4 and MMC_5 are at their minima when $U_{W2} = 0.98$ pu. Since the x_O of $\mathrm{Q}_{\mathrm{MMC2}}$ reaches an acceptable value, which is near its minimum value, at $U_{W2} = 0.98$ pu, the over-correction of $\mathrm{Q}_{\mathrm{MMC2}}$ does not noticeably impact the system during the transient event.

Fig. 9(c) and (d) show that at $U_{W2} = 0.98$ pu, the DC voltages and DC currents can obtain their minimum values of x_O. This indicates that MMC_1, MMC_2, MMC_4 and MMC_5 can achieve the smallest over-corrections in DC voltages and currents, if U_{W2} is selected at 0.98 pu.

TABLE V
ADJUSTMENT-TIME AND NEW STEADY STATE DC VOLTAGE OF MMC_1

U_{S4} (pu)	0.94	0.95	0.96	0.97	0.98
Adjustment-time (s)	36.78	35.45	32.98	33.73	49.08
New Steady State U_{dc} (pu)	0.9716	0.9716	0.9716	0.9716	0.9785

Similar studies to those of Fig. 9 are also conducted for the electrical variables of the ten synchronous machines of Fig. 6, i.e., active and reactive power and rotor speed of each generator. The study results also show that 19 out of the 30 electrical variables of the generators exhibit their smallest x_O at $U_{W2} = 0.98$ pu. It should be noted that out of the 16 electrical variables of Fig. 9, 14 reach to their minimum x_O values at $U_{W2} = 0.98$ pu. The reported observations based on this trial and error approach indicates that $U_{W2} = 0.98$ pu for MMC_2 results in minimum impact on the system behavior subsequent to a transient scenario, and thus this is a desirable threshold value for the engage region of the droop-control of MMC_2.

- Case IV – Selection of U_{S4}

U_{S4} is the lower threshold of the disengage region of MMC_1. Table V reports the adjustment-time and the new steady-state DC voltage of MMC_1 when U_{S4} is changed from 0.94 to 0.98 pu. The criterion that used to identify MMC_1 reach a new steady state is that the oscillation of each electric variable of MMC_1 is confined within 0.5% of its new steady sate value.

Table V shows that for $U_{S4} = 0.98$ pu, the new steady-state U_{dc} is 0.9785 pu which is lower than U_{S4}. This indicates the droop-control of MMC_1 is activated to obtain the new steady-state DC voltage. Since the lower threshold value of the disengage region of MMC_2 is 0.99 pu, the droop-control of MMC_2 is also activated as shown in Fig. 7(a). The interactions of droop-controls of MMC_1 and MMC_2 result in the adjustment-time of 49.08 s and higher new steady-state DC voltages for the MMCs in service.

When $U_{S4} = 0.94$ pu, the disengage region is very close to the engage region, i.e., U_{W4} is 0.935 pu, and thus the DC voltage may repeatedly change between the two close threshold limits during transients and cause a longer adjustment-time. One approach for solving this problem is to select a proper voltage difference between the two threshold values. Interactions of the droop-controls of the MMCs make the updated steady-state DC voltage closer to the original one and result in a longer adjustment-time. The threshold values of a dead-band can be determined for a lower over-correction, a shorter adjustment-time and a proper new steady state DC voltage.

VI. CONCLUSION

This paper presents an enhanced droop-based DC voltage control method, including dead-band, for the VSC-HVDC grid applications. The proposed approach imposes the net-zero AC-DC power balance for the HVDC grid and utilizes an improved power-voltage characteristic to achieve desirable dynamic per-

formance for each VSC station. The main features of the proposed droop-based voltage control include: (i) dividing the converter stations into four groups, (ii) assigning each group with a unique voltage margin and dead-band to activate/deactivate the proposed droop-control and (iii) providing an improved power-voltage characteristic to adjust the new steady-state DC voltages of the VSCs closer to their pre-disturbance values. This paper elaborates on an approach to determine each dead-band to reduce the over-corrections and shortens the adjustment-time of the electrical variables subsequent to transient events.

This paper also presents a method to determine the dead-bands to alleviate the impact of transient events on the operating points of converter stations. The salient feature of the proposed droop-control method is that it does not require retuning the voltage margins and dead-bands as the number of HVDC stations, due to the in- or out-of-service modes of converters, changes. A set of time-domain simulation studies, using the PSCAD software tool, were conducted on a five-terminal VSC-HVDC grid to demonstrate the feasibility and effectiveness of the proposed control method for the HVDC grid applications.

REFERENCES

[1] N. Flourentzou, V. G. Agelidis, and G. D. Demetriades, "VSC-based HVDC power transmission systems: An overview," *IEEE Trans. Power Electron.*, vol. 24, no. 3, pp. 592–602, May 2009.

[2] W. Lu and B. T. Ooi, "DC overvoltage control during loss of converter in multi-terminal voltage-source converter-based HVDC (M-VSC-HVDC)," *IEEE Trans. Power Del.*, vol. 18, no. 3, pp. 915–920, Jul. 2003.

[3] O. Gomis-Bellmunt, J. Liang, J. Ekanayake, and N. Jenkins, "Voltage-current characteristics of multi-terminal HVDC-VSC for offshore wind farms," *Elect. Power Syst. Res.*, vol. 81, no. 2, pp. 440–450, Feb. 2011.

[4] M. Saeedifard and R. Iravani, "Dynamic performance of a modular multilevel back-to-back HVDC system," *IEEE Trans. Power Del.*, vol. 25, no. 4, pp. 2903–2912, Oct. 2010.

[5] H. Li *et al.*, "A start strategy for synchronized connections of MMCs to an AC system," *Int. J. Elect. Power Energy Syst.*, vol. 69, pp. 380–390, Jul. 2015.

[6] C. Liu *et al.*, "Sub-module component developed in C-Builder for MMC control and protection test in RTDS," *Int. J. Elect. Power Energy Syst.*, vol. 56, pp. 198–208, Mar. 2014.

[7] D. V. Hertem and M. Ghandhari, "Multi-terminal VSC-HVDC for the European supergrid: Obstacles," *Renew. Sustain. Energy Rev.*, vol. 14, no. 9, pp. 3156–3163, Dec. 2010.

[8] J. Cao and J. Y. Cai, "HVDC in China," presented at the EPRI, HVDC & FACTS Conf., Palo Alto, CA., USA, Aug. 2013.

[9] T. K. Vrana *et al.*, "A classification of DC node voltage control methods for HVDC grids," *Elect. Power Syst. Res.*, vol. 103, pp. 137–144, Oct. 2013.

[10] F. B. Ajaei and R. Iravani, "Dynamic interactions of the MMC-HVDC grid and its host AC system due to AC-side disturbance," *IEEE Trans. Power Del.*, vol. 31, no. 3, pp. 1289–1298, Jun. 2016.

[11] E. Prieto-Araujo, F. D. Bianchi, A. Junyent-Ferre, and O. Gomis-Bellmunt, "Methodology for droop control dynamic analysis of multi-terminal VSC-HVDC grids for offshore wind farms," *IEEE Trans. Power Del.*, vol. 26, no. 4, pp. 2476–2485, Oct. 2011.

[12] R. T. Pinto *et al.*, "A novel distributed direct-voltage control strategy for grid integration of offshore wind energy systems through MTDC network," *IEEE Trans. Ind. Electron.*, vol. 60, no. 6, pp. 2429–2441, Jun. 2013.

[13] J. Beerten and R. Belmans, "VSC-MTDC systems with a distributed DC voltage control—A power flow approach," in *Proc. IEEE PowerTech*, Trondheim, Norway, Jun. 2011, pp. 1–6.

[14] R. E. Torres-Olguin *et al.*, "Experimental verification of a voltage droop control for grid integration of offshore wind farms using multi-terminal HVDC," *Energy Procedia*, vol. 53, pp. 104–113, Jul. 2014.

[15] C. Dierckxsens *et al.*, "A distributed DC voltage control method for VSC-MTDC systems," *Elect. Power Syst. Res.*, vol. 82, no. 1, pp. 54–58, Jan. 2012.

[16] T. K. Vrana, L. Zeni, and O. B. Fosso, "Dynamic active power control with improved undead-band droop for HVDC system," in *Proc. 10th IET Int. Conf. AC DC Power Transmission*, Birmingham, U.K., Dec. 2012, pp. 1–6.

[17] C. Guo and C. Zhao, "A new technology for HVDC start-up and operation using VSC-HVDC system," in *Proc. IEEE Power & Energy Soc. General Meeting*, Calgary, AB, Canada, Jul. 2009, pp. 1–5.

[18] H. Li *et al.*, "Design of defined controller for modular multilevel converter based on CPS-SPWM in PSCAD," in *Proc. IEEE Power & Energy Soc. General Meeting*, Denver, CO, USA, Jul. 2015, pp. 1–5.

[19] CIGRE WG B4–37, "VSC transmission," Rep. 269, Apr. 2005.

[20] D. Rai *et al.*, "Damping inter-area oscillations using phase imbalanced series compensation schemes," *IEEE Trans. Power Syst.*, vol. 26, no. 3, pp. 1753–1761, Aug. 2011.

[21] T. Athay, R. Podmore, and S. Virmani, "A practical method for the direct analysis of transient stability," *IEEE Trans. Power App. Syst.*, vol. PAS-98, no. 2, pp. 573–584, Mar./Apr., 1979.

Haifeng Li (S'13) received the B.S. and M.S. degrees from the School of Electrical and Electronic Engineering, North China Electric Power University, Beijing, China. He is currently a doctoral program student at the School of Electrical and Electronic Engineering, North China Electric Power University. His current interest includes operation strategy for the MMC-HVDC system. He has been at the University of Toronto since September 1, 2015, as a Visiting Ph.D. Student.

Chongru Liu (M'10–SM'15) received the B.S., M.S., and Ph.D. degrees in E.E. from Tsinghua University, Beijing, China. She is an Associate Professor in the School of Electrical and Electronic Engineering, North China Electric Power University, Beijing, China. Her current interests include analysis, operation, and control of ac/dc system.

Dr. Liu is currently a Member of the Nation Power System Management and Information Exchange Standardization Committee of China.

Gengyin Li (M'03) was born in Hebei Province, China. He received the B.S., M.S., and Ph.D. degrees, all in electrical engineering, from North China Electric Power University, Beijing, China. Since 1987, he has been with the School of Electrical and Electronic Engineering at NCEPU, where he is currently a Professor and Executive Vice Dean of the School. His research interests include power system analysis and reliability, power quality analysis and control, HVDC and VSC-HVDC transmission technology, and power systems economics.

Reza Iravani (M'85–SM'00–F'03) received the B.Sc. degree in electrical engineering from Tehran Polytechnic University, Tehran, Iran, in 1976, and the M.Sc. and Ph.D. degrees in electrical engineering from the University of Manitoba, Winnipeg, MB, Canada, in 1981 and 1985, respectively. Currently, he is a Professor with the Department of Electrical and Computer Engineering, University of Toronto, Canada. His research interests include power electronics and power system dynamics and control.